Nanoscale Res Lett (2010) 5:1570–1577
DOI 10.1007/s11671-010-9678-y

NANO EXPRESS

An Antireflective Nanostructure Array Fabricated by Nanosilver Colloidal Lithography on a Silicon Substrate

Seong-Je Park · Soon-Won Lee · Ki-Joong Lee · Ji-Hye Lee · Ki-Don Kim · Jun-Ho Jeong · Jun-Hyuk Choi

Received: 29 March 2010 / Accepted: 29 June 2010 / Published online: 14 July 2010

Abstract An alternative method is presented for fabricating an antireflective nanostructure array using nanosilver colloidal lithography. Spin coating was used to produce the multilayered silver nanoparticles, which grew by self-assembly and were transformed into randomly distributed nanosilver islands through the thermodynamic action of dewetting and Oswald ripening. The average size and coverage rate of the islands increased with concentration in the range of 50–90 nm and 40–65%, respectively. The nanosilver islands were critically affected by concentration and spin speed. The effects of these two parameters were investigated, after etching and wet removal of nanosilver residues. The reflection nearly disappeared in the ultraviolet wavelength range and was 17% of the reflection of a bare silicon wafer in the visible range.

Keywords Antireflective · Nanosilver · Nanostructure · Nanoislands · Colloidal lithography

Introduction

The demand for an effective fabrication method for a large-area nanostructure array has recently stimulated increased interest and research activities in the fields of optics and optoelectronics, including photovoltaic cells, light-emitting devices, and photo-detectors. Two-dimensional arrays of nanostructures have been reported to enable modulation of both the energy and the path of photons to increase efficiency and sensitivity [1–3] while also providing antireflective properties. The antireflective property improves the visibility of the transparent window, as well as the light extraction or absorption efficiency, by reducing the reflection of incident light and increasing its transmission accordingly. In fact, the reflectivity can be greatly suppressed for a wide spectral bandwidth when a nanostructure array with a subwavelength pitch can make a continuous and monotonous change in the effective refractive index from air to the solid surface [4–6]. Stability problems due to the thermal mismatch in the conventional methods applying multilayered thin films [5, 7] can be improved.

The previous fabrication strategy relied on costly e-beam lithography [7], whereas molding technologies, such as nanoimprinting, have emerged due to high throughput and cost-effective process capabilities [5, 8–16]. Master patterns required for molding can be fabricated by e-beam [5], interference lithography [8, 9], anodizing aluminum oxide [10, 11], colloidal nanolithography using polystyrene [12–14], and electron cyclotron resonance (ECR) plasma etching [15, 16]. Although molding technology is favorable for mass production, the high cost of mask preparation and the limited resources for large-area mask patterning frequently restrict its practical applications.

Simpler bottom-up fabrication using a molding stamp with a subwavelength nanostructure array can be achieved through thermal dewetting of a metal film. Sputter-coated metal film is transformed into an isolated random array of metal dots when thermally annealed, which can be used as the etch shadow mask for the following substrate etching to make an antireflective nanostructure array. Thermal dewetting of Pt/Pd alloy film on a Si wafer was previously studied for this purpose [17]. Other previous attempts

S.-J. Park · S.-W. Lee · K.-J. Lee · J.-H. Lee · K.-D. Kim · J.-H. Jeong · J.-H. Choi (✉)
Department of Nanomechanical System, Korea Institute of Machinery and Materials, 171 Jang-dong, Yuseung-gu, Daejeon, Republic of Korea
e-mail: junhyuk@kimm.re.kr

include thermal dewetting of Ni film on a SiO_2 surface [18], Ag sputtering on a heated surface [19], and Ag sputtering followed by thermal dewetting on a curved surface [20]. The transformation results from the increased surface energy of the metal film and its subsequent move to a minimum energy state, similar to the principle of Ostwald ripening [21, 22]. This approach has more promise for large-area process applications in view of enhanced uniformity and fewer defects compared to the colloidal lithography commonly with polystyrene nanoparticles [23, 24], which yields more defects and pattern irregularities as the substrate size increases. However, the vacuum deposition and high process temperatures (greater than 300 °C) used to increase the surface energy of the metal can often limit its applications and are unfavorable for polymer-coated substrates.

In this paper, we report an alternative method for fabricating an etch mask with a subwavelength nanostructure array for antireflective applications using nanosilver colloids and relatively low annealing temperatures. As-received nanosilver colloids with diameters of 20–30 nm were agglomerated into isolated nanosilver islands on a wafer-scale silicon substrate in the range of 50–80 nm via a combined mechanism of solvent dewetting and Ostwald ripening using spin coating and substrate heating. Several variables were identified, including nanosilver density, spin coating speed, nanosilver colloid size, annealing temperature, and time, to vary the size and coverage rate of the nanosilver islands. Due to the sufficiently high etch selectivity of silver to silicon, various configurations and aspect ratios of nanostructures could be easily achieved. Pillar-like nanostructures resulted, and their heights varied proportionally with etch time. The reflection rate was reduced below 5%, which is much lower than the 40% of bare silicon in the visible zone. In particular, the reduction effect of reflection was maximized in the ultraviolet (UV) region of ~300 nm with a rate of over 95%.

Experimental

As-received nanosilver colloidal ink (InkTech Inc., Korea), which include nanosilver particles in the range of 10–30 nm dispersed in a non-polar solvent blend (xylene, ethylene glycol, and others; the exact information was confidential to InkTech Inc.), was diluted to 1–10 wt% using the product-customized thinner. Its images were analyzed by transmission electron microscopy (TEM; Fig. 1). The deposition and transformation process into nanosilver islands was presumed to proceed according to diagram shown in Fig. 2. Nanosilver colloidal ink was spin-coated onto a full wafer-scale silicon substrate to form

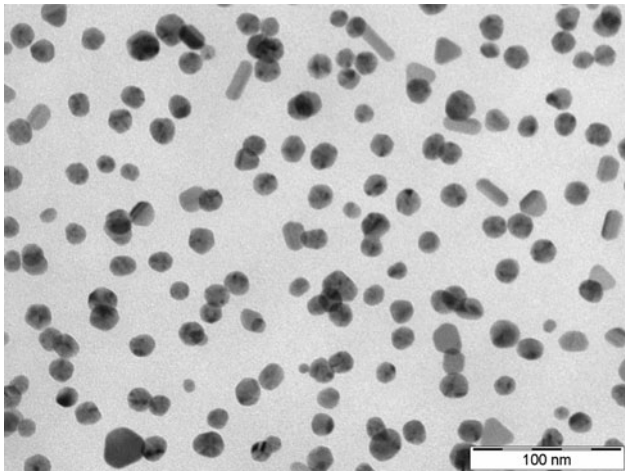

Fig. 1 TEM image of as-received silver nanoparticles

a multilayered nanosilver film (Fig. 2a) and transformed to an isolated random array of nanosilver islands by thermal annealing during the following steps. Figure 2b shows the multilayered film of nanosilver particles in its initial wet state. It begins to be dewetted as the temperature increases. The continuous film is broken off and grows with increasing space between neighboring islands (Fig. 2c). Ultimately, the nanosilver islands are completely solidified (Fig. 2d). This process is affected by several parameters, including the as-received particle size, type of solvent, concentration, spin speed, annealing temperature, and time. In this work, the average size and coverage rate (density) of the nanosilver islands were analyzed using concentrations from 3 to 7 wt%, and spin speeds in the range of 2,000–4,000 rpm with other fixed conditions of annealing temperature (250 °C) and time (15 min). The initial annealing temperature was set at 180 °C, lower than nanosilver sintering temperature (250 °C), to prevent instantaneous sintering of nanosilver before sufficient dewetting occurred.

The antireflective nanostructure array was fabricated via reactive ion etching (Multiplex ICP—STS, Oxford Systems) with the optimized condition of C_4F_8 (40 sccm) and SF_6 (45 sccm), following a wet removal process of nanosilver residues to form a pattern array of nanosilver islands as an etch mask. Various structural configurations of the nanopillar array were flexibly achievable due to good etch selectivity of silver to silicon. Allowing slight isotropic etching condition, the etching condition was optimized to fit into the aspect ratio of one at the present approach, if etching is done for 60 s under the given conditions. Finally, the reflectance from the ultraviolet to the visible region was measured by UV spectroscopy (Model: Varian Cary 5000) at the incidence angle of 7°, located in the OLED center of Seoul National University in Korea. The light source was tungsten–halogen for the visible region and deuterium for

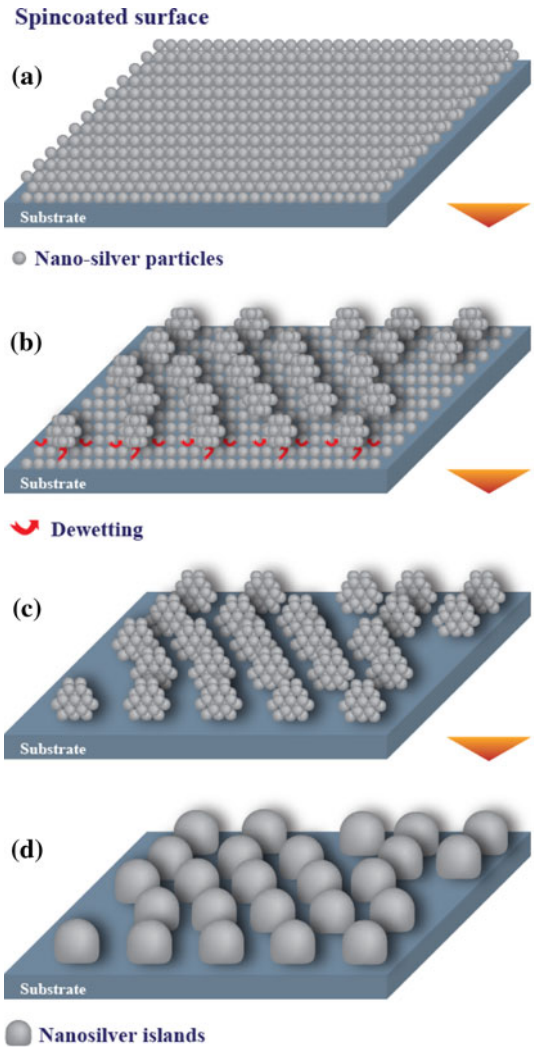

Fig. 2 Fabrication schematic of nanosilver islands for an antireflective etch mask

the ultraviolet region. The antireflective effects for the two most dominant process conditions, concentration and spin speed, were investigated for nanopillar structures with an aspect ratio close to one.

Results and Discussion

The transformation of multilayered nanosilver film into an isolated random array of nanosilver islands was most likely thermodynamically driven by the combined self-assembly of dewetting and Ostwald ripening. Heating the plate made the surface energy of the solvent and nanosilver increase, causing microscopic dewetting of the solvent with tiny nanosilver particles captured inside a dewet droplet. Further increasing the plate temperature to 250 °C, increased the agglomeration of nanosilver islands due to self-assembly. Finally, the islands were sintered to create a randomly distributed array of nanosilver islands during the extended heating stage. In this process, the surface energy of the applied solvent in the nanosilver ink is the most critical factor controlling the transformation. Comparison of the three images in Fig. 3 shows the transformation is completed with the use of a non-polar solvent blend at 3 wt% of nanosilver (Fig. 3a), while silver colloids dispersed in isopropyl alcohol (IPA) did not complete the transformation (Fig. 3b, c) since the polar solvent was quite volatile due to the relatively low surface energy compared to non-polar counterparts. The results of the comparison justify the transformation mechanism described earlier.

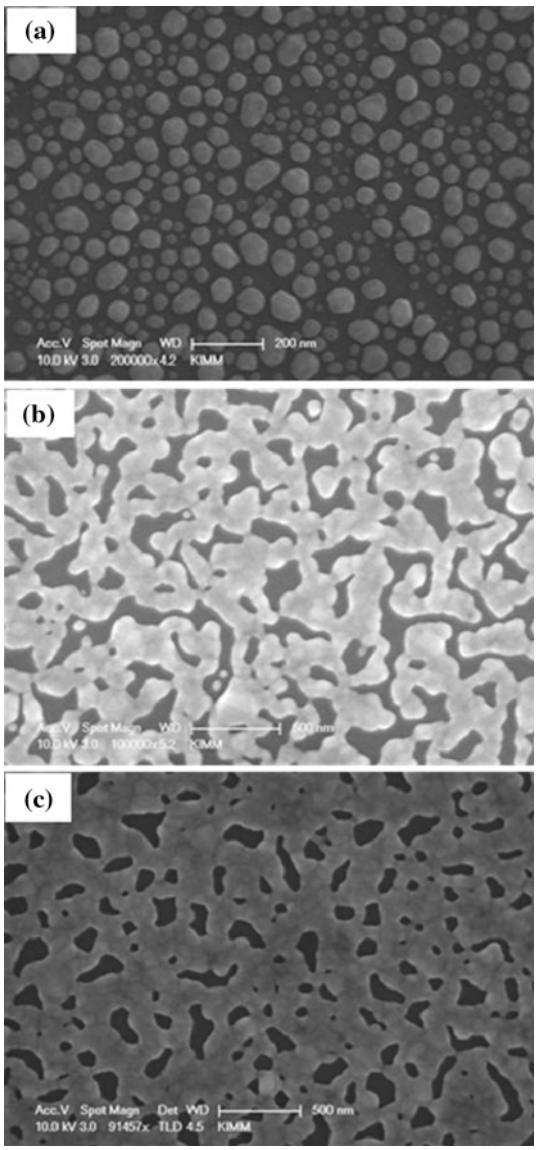

Fig. 3 Effect of the nanosilver colloidal solvent on the nanosilver island transformation: **a** 3 wt% in non-polar solvent including xylene, etc., **b** 5 wt% in IPA (polar solvent), **c** 5 wt% in IPA

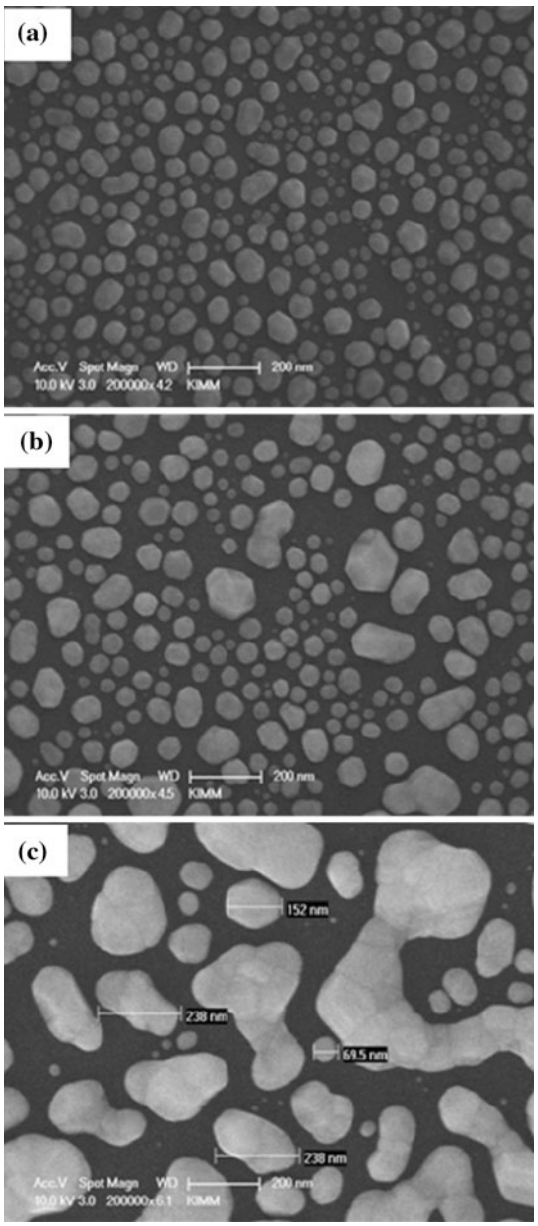

Fig. 4 Nanosilver island size and configuration in terms of Ag concentration (4,000 rpm applied): **a** 3 wt%, **b** 5 wt%, **c** 7 wt%

The effects of nanosilver concentration and spin speed on the formation of nanosilver islands are presented in Figs. 4 and 5, respectively. As the nanosilver concentration increased from 3 to 7 wt% at a spin speed of 4,000 rpm, the size of the nanosilver islands increased accordingly. The nanosilver islands began to form networks with the neighboring nanosilver islands above 7 wt%. Increasing the spin speed reduced the average size of the islands, as shown in Fig. 5. These results imply that the thickness of the as-coated nanosilver multilayer determines the average size of the nanosilver islands proportionally.

A quantitative analysis was performed to more clearly define the effects of the nanosilver islands on the average

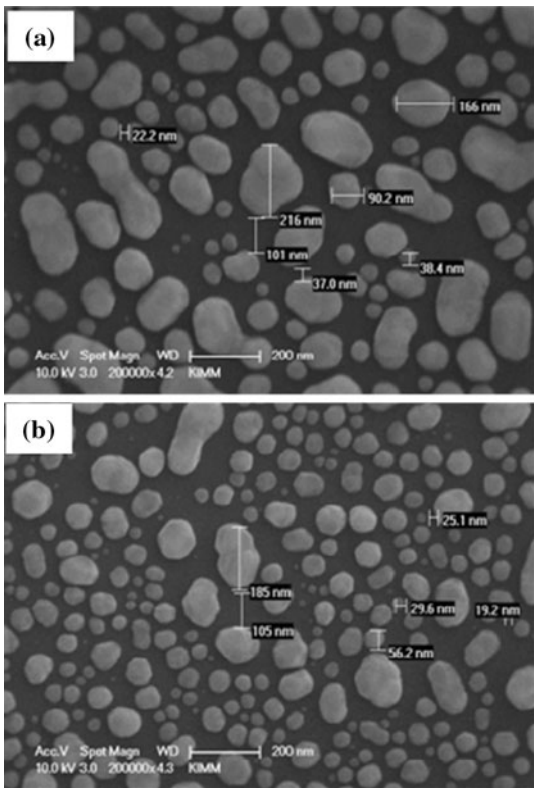

Fig. 5 Effect of spin speed on the nanosilver deposition for 5 wt%: **a** 2,000 rpm, **b** 4,000 rpm

size and coverage rate in Fig. 6 and Table 1. The average size increased from 58.1 nm for 3 wt% to 62.6 nm for 5 wt% by a rate of 7.7% at a spin speed of 4,000 rpm, whereas the average size increased from 69.5 nm to 79.3 nm by a rate of 14.1% at 2,000 rpm in the central region. Increased rate grows up to be 37.7, 45.9% at 4,000 and 2,000 rpm, respectively at the outer region as shown in Table 1. These results suggest the effect of nanosilver concentration gets more critical at lower spin speed, and outer side along with the increased standard deviation, which implies the areal uniformity is limited in the spin-coated substrate. In comparison, on the other hand, the spin speed seems to be more effective to grow up the average size of nanosilver islands. The increase rates of 19.6 and 26.7% were driven when the spin speed reduces from 4,000–2,000 rpm for 3 and 5 wt%, respectively. For all cases, the standard deviation shows similar tendency to the average size of nanosilver islands with respect to nanosilver concentration and spin speed. It should be noted that in the present investigation, the smaller islands, less than roughly 30 nm, were not counted because they were lifted off during the following substrate etching and did not remain in the final etched nanostructure array. Under the given analysis conditions, the coverage rate increased in proportion to the nanosilver concentration and spin speed

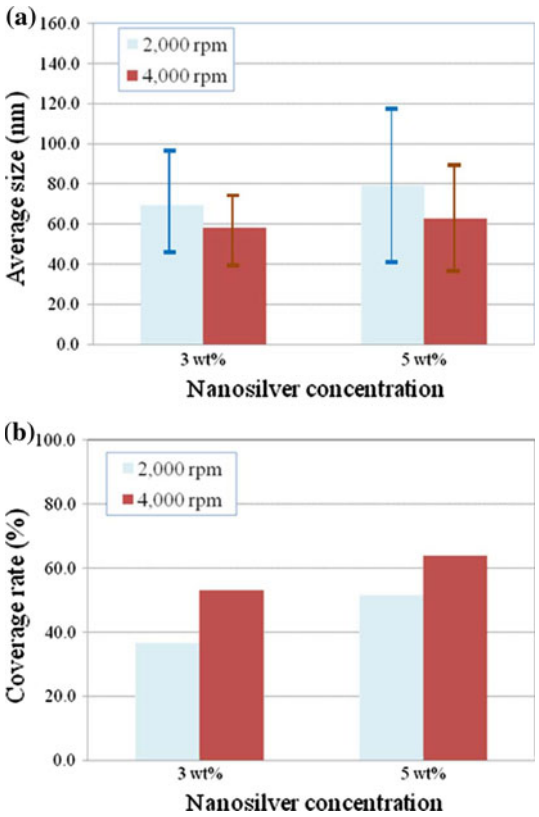

Fig. 6 Quantitative analysis of nanosilver islands in terms of the concentration and spin speed: **a** average size, **b** coverage rate

as well. It was expected that further grown nanosilver islands would expose more open spaces to the substrate as the nanosilver concentration increased. However, the coverage rate is also directly related to the standard deviation of the island size, which is likely to reduce with increased spin speed because the higher spin speed improves the uniformity of the film. Therefore, the lower spin speed creates a wider spectrum of the island size with an even greater number of smaller islands than were counted in this analysis, even though the lower speed generates a larger average size. This explains why the coverage rate increased with the spin speed.

Figure 7 shows photographs of both the nanosilver-coated etch mask (top) and the etched substrate (bottom). The etch mask colors were nearly the same as the bare

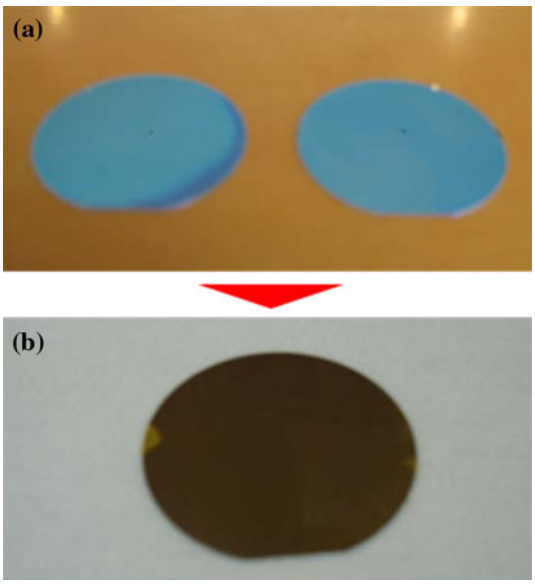

Fig. 7 Full wafer-scale view of the **a** nanosilver island deposited wafer and **b** etched wafer

wafer, whereas the etched substrate showed a color change to dark with considerably diminished reflection. Figure 8 shows SEM images of the etched nanostructure array as a function of etch time (40 and 60 s) for the samples processed at a spin speed of 2,000 rpm and nanosilver concentration of 5 wt%. The higher nanostructure pillars (~110 nm) were surely obtained as the etch time was extended to 60 s (Fig. 8b). These SEM images validate that the smaller islands, less than roughly 30 nm, tends to be lift-off during etching. Hence, the etching under the given condition creates cone-shaped nanopillars for the etch mask of nanosilver islands in the range of roughly 30–60 nm, the depth of which is in proportion to the size of nanosilver islands. This can provide the chances of a continuous and monotonous change in the effective refractive index from air to the solid surface for the reduced light reflections. This also can explain that the nanosilver islands in Fig. 8(b-2) looks close to completely isolated circles relatively in comparison with Fig. 8(a-2), due to etching condition accompanying lift-off.

The reflective properties of the finalized nanostructure arrays on the silicon substrate were measured in the

Table 1 Quantitative analysis of nanosilver islands in different zone of the deposited wafer

Spin speed (rpm)	Nanosilver concentration (wt%)	Center			Periphery		
		Ave. (nm)	SD (nm)	Coverage (%)	Ave. (nm)	SD (nm)	Coverage (%)
2,000	3	69.5	27.0	36.5	63.3	19.3	44.9
	5	79.3	37.1	51.6	92.4	52.9	64.0
4,000	3	58.1	17.9	53.2	47.7	11.2	46.0
	5	62.6	28.8	64.0	65.7	29.4	65.2

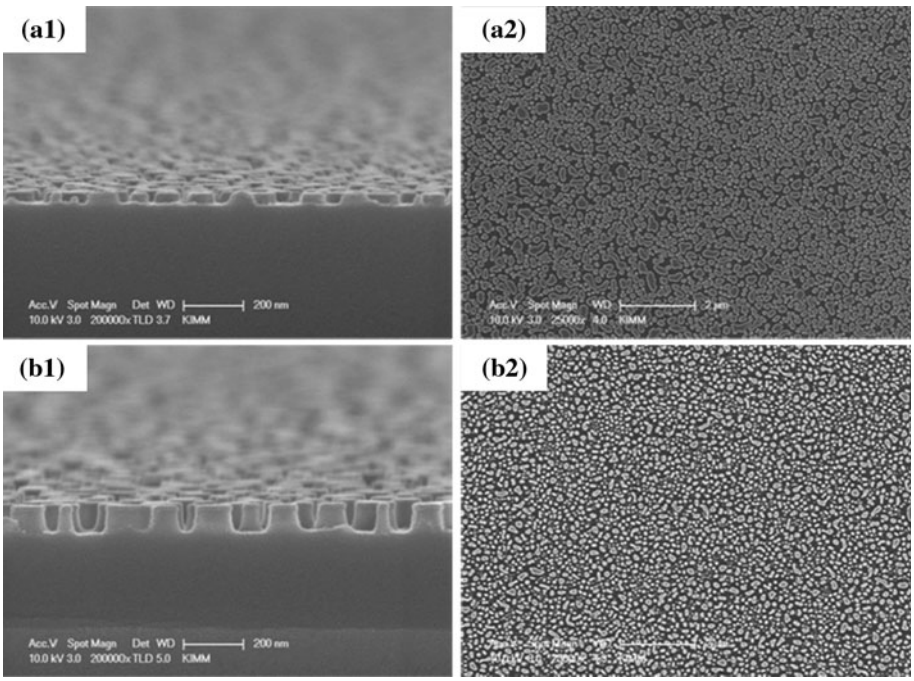

Fig. 8 Antireflective nanostructure array after etching and removal of nanosilver residues for the samples processed at 2,000 rpm and 5 wt%: etch time of **a** 40 s, **b** 60 s

UV–visible region (Fig. 9) for the etched samples (40 and 60 s) to investigate the effect of etched depth. Compared to the bare silicon wafer, the reflections of the array were greatly reduced depending on the process conditions (spin speed and concentration) of the nanosilver island fabrication and etched depth.

The highest antireflection occurred at the higher concentration (5 wt%) and for the extended etch time in Fig. 9b, which indicates that the larger size and higher nanopillar arrays were more effective at reducing the reflection. The minimum reflection rate in Fig. 9b decreased to about 0.7% around a wavelength of 300 nm in the UV region, and 5–6% in the visible region. The antireflection rate, compared to the bare silicon wafer, was approximately 98 and 83% in the UV and visible regions, respectively for the given condition. Hence, the antireflection turned out to be more dominant in the UV region, probably because the achieved average size of the nanosilver islands (50–90 nm in the present experiments) was more suitable to interact with the UV than in the visible light rays. This agrees with the result that the reflection reduction rate varied with the nanosilver concentration and spin speed in Fig. 9. The second primary factor to affect the reflection is the nanostructure height shown in comparison of Fig. 9a, b. The minimum reflection rate in Fig. 9a, where the etched depth is around 50 nm, is about 10% in the visible region for 5 wt% concentration with the doubled antireflection efficiency from in Fig. 9b. Furthermore, the reflection data band for the given conditions apparently gets larger along with the etched depth in Fig. 9b, which is assumingly due to increasing occurrence of lift-off during etching especially for '3 wt%-4,000 rpm', the coating process condition of the smallest size of nanosilver island array.

An additional minor factor to influence the reflection of silicon substrate may be the coverage rate (nanopillar density). In comparison of 'Ag 5 wt%-4,000 rpm' with 'Ag 3 wt%-2,000 rpm' in Fig. 9b, the anti-reflection effect is greater for 'Ag 5 wt%-4,000 rpm' although its average size of nanosilver islands is smaller than 'Ag 3 wt%-2,000 rpm'. This probably results from the higher coverage rate in 'Ag 5 wt%-4,000 rpm' than in 'Ag 3 wt%-2,000 rpm'. It represents that the density of nanopillar array is higher for 'Ag 5 wt%-4,000 rpm', which leads to the larger effect of anti-reflection than 'Ag 3 wt%-2,000 rpm'. The reversed result in Fig. 9a seems to be due to the unexpected data deviation all within the limited range of tolerable inaccuracy, which always comes up for random self-assembly. Further study would be required to more clearly identify and improve the antireflection efficiency.

Conclusion

We investigated an alternative method to fabricate a wafer-level antireflective nanostructure array using nanosilver colloidal lithography. The combined action of dewetting and Oswald ripening contributed to the transformation of the spin-coated multilayer of nanosilver colloids into randomly

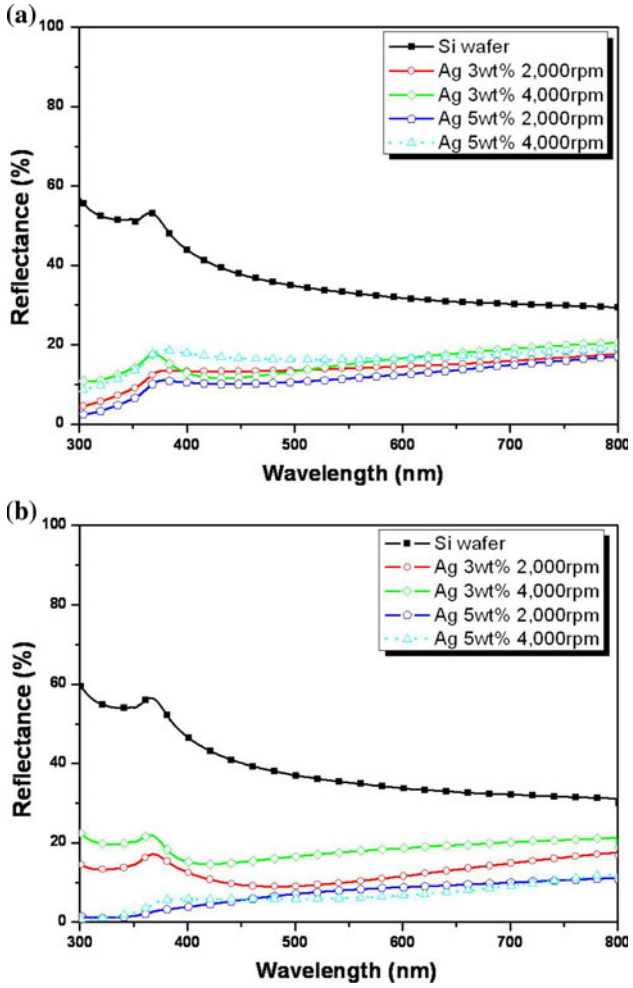

Fig. 9 Reflection rates for the nanostructured samples with a bare silicon wafer as a reference: **a** the etched for 40 s, **b** the etched for 60 s

distributed nanosilver islands that could be used as an etch mask for antireflective nanostructures. Accordingly, the spin-coated nanosilver colloidal layer began to be dewetted and agglomerate as it gradually solidified from its wet state under various annealing conditions. Finally, the nanosilver islands grew and sintered at their sintering temperature. From five identified process parameters, the average size and coverage rate of the nanosilver islands were affected most critically by the concentration and the spin speed. The as-received colloid size, temperature, and annealing time were less critical parameters. The average size of the resulting nanosilver islands was in the range of 50–100 nm, with a coverage rate of 40–60% and the standard deviation of 20–50%. It may not be at the acceptable level in many applications other than nanostructured optics such as antireflection window in which such randomness is even ideal to cover a wide range of wavelength spectrum.

Compared with sputter-coated metal film, reported previously [17–20], the colloidal form is more readily viscous at relatively lower temperatures. Additionally, the solvent wet state at the beginning of the temperature increase can facilitate dewetting and agglomerating of metal colloids into the isolated islands. Hence, the present approach may provide an improved method for a more effective self-assembled transformation. The wet process and low temperature annealing are advantages of the present process for extended process applications.

Etching through silicon substrates produced various structural profiles and nanopillar heights as a function of etch time. Anisotropic etching was performed to generate a nanopillar profile with nearly right-angled edges. The reflection measurements revealed that the antireflection effect was substantially large in general, and depends on the nanopillar height. The reflection nearly disappeared in the UV wavelength range and was only 17% of that of a bare silicon wafer in the visible range for the condition of the extended etch time and largest nanosilver concentration that turned out to be ideal process theme for this approach. The present data level for the antireflection rate is comparable with those reported in previous publications [17, 19].

The present fabrication method is expected to draw extensive industrial interest for producing large-area nanotemplates in a cost-effective and more accessible manner. Nanosilver island arrays could also be used for other optoelectronic applications to improve performance. For example, the array could be used as a metal dot layer to derive localized surface plasmon resonance (LSPR)-coupled light emission [25, 26]. More in-depth understanding and further investigation of the nanosilver island transformation would improve the uniformity, process stability, and throughput.

Acknowledgments This research was supported by a grant (08K1401-00511) from the Center for Nanoscale Mechatronics and Manufacturing, one of the 21st Century Frontier Research Programs, and a Platform Project grant (10033636-2009-11) supported by the Ministry of the Knowledge Economy of Korea.

References

1. S.H. Jeon, J.W. Kang, H.D. Park, J.J. Kim, J.R. Youn, J.Y. Shim, J.H. Jeong, D.G. Choi, K.D. Kim, A.O. Altun, S.H. Kim, Y.H. Lee, Appl. Phys. Lett. **92**, 223307 (2008). doi:10.1063/1.2939554
2. F.C. Diana, A. David, I. Meinel, R. Sharma, C. Weisbuch, S. Nakamura, P.M. Petroff, Nano Lett. **6**, 1116 (2006). doi: 10.1021/nl060535b
3. K.Y. Yang, K.C. Choi, C.W. Ahn, Opt. Exp. **17**, 11495 (2009)

4. E.B. Grann, M.G. Moharam, D.A. Pommet, J. Opt. Soc. Am. **A12**, 333 (1995). doi:10.1364/JOSAA.12.000333
5. Y. Kanamori, E. Roy, Y. Chen, Microelectron. Eng. **78**, 287 (2005). doi:10.1016/j.mee.2004.12.039
6. H. Kobayashi, N. Moronuki, A. Kaneko, Int. J. Precis. Eng. Manuf. **9**, 25 (2008)
7. Y. Kanamori, M. Sasaki, K. Hane, Opt. Lett. **24**, 1422 (1999). doi:10.1364/OL.24.001422
8. C.J. Ting, C.F. Chen, C.P. Chou, Opt. Commun. **282**, 434 (2009). doi:10.1016/j/optcom.2008.10.026
9. X.Z. Chen, H.Y. Li, Chin. Phys. Lett. **24**, 2830 (2007). doi:10.1088/0256-307x/24/10/032
10. H.S. Hong, H.S. Han, H. Lee, J.U. Cho, Y.G. Kim, Jpn. J. Appl. Phys. **46**(9B), 6375 (2007). doi:10.1143/jjap.46.6375
11. Y.S. Kim, K.M. Lee, J.S. Lee, G.Y. Jung, W.B. Kim, Nanotechnology **19**, 365305 (2008). doi:10.1088/0957-4484/19/36/365305
12. B.H. Wang, W. Zhao, A. Chen, S.J. Chua, J. Crystal Growth **288**, 200 (2006). doi:10.1016/j.jcrysgro.2005.12.051
13. W.L. Xu, W.M. Zhao, P. Sun, X.F. Huang, K.J. Chen, Appl. Surf. Sci. **253**, 9035 (2007). doi:10.1016/j.apsusc.2007.05.024
14. Y.H. Kang, S.S. Oh, Y.S. Kim, C.G. Choi, Microelectron. Eng. **87**, 125 (2010). doi:10.1016/j.mee.2009.06.006
15. J. Shieh, C.H. Lin, M.C. Yang, J. Phys. D Appl. Phys. **40**, 2242 (2007). doi:10.1088/0022-3727/40/8/S02
16. C.J. Ting, M.C. Huang, H.Y. Tsai, C.P. Chou, C.C. Fu, Nanotechnology **19**, 205301 (2008). doi:10.1088/0957-4484/19/20/205301
17. Y.J. Lee, K.S. Koh, H.J. Na, K.O. Kim, J.J. Kang, J.B. Kim, Nano. Res. Lett. **4**, 364 (2009). doi:10.1007/sl1671-009-9255-4
18. G.R. Lin, Y.C. Chang, E.S. Liu, H.C. Kuo, H.S. Lin, Appl. Phys. Lett. **90**, 181923 (2007). doi:10.1063/1.2736281
19. S. Wang, X.Z. Yu, H.T. Fan, Appl. Phys. Lett. **91**, 061105 (2007). doi:10.1063/1.2767990
20. K. Kurihara, Y. Saitou, T. Nakano, H. Kato, Tominaga, International Display Workshop FMC6-1 (2007)
21. P. Sharma, C.Y. Liu, C.F. Hsu, Appl. Phys. Lett. **89**, 163110 (2006). doi:10.1063/1.2355475
22. P.L. Redmond, A.J. Hallock, L.E. Brud, Nano Lett. **5**, 131 (2005). doi:10.1021/nl048204r
23. C.L. Cheung, R.J. Kikolic, C.E. Reinhardt, T.F. Wang, Nanotechnology **17**, 1339 (2006). doi:10.1088/0957-4484/17/5/028
24. M.J. Huang, C.R. Yang, Y.C. Chiou, R.T. Lee, Sol. Energy Mater. Sol. Cell **92**, 1352 (2008). doi:10.1016/j.solmat.2008.05.014
25. D.M. Yeh, C.F. Huang, C.Y. Chen, Y.C. Lu, C.C. Yang, Nanotechnology **19**, 34501 (2008). doi:10.1088/0957-4484/19/34/345201
26. M.K. Kwon, J.Y. Kim, B.H. Kim, I.K. Park, C.Y. Cho, C.C. Byeon, S.J. Park, Adv. Mater. **20**, 1253 (2007). doi:10.1002/adma.200701130